Systematic Interrogation of Tumor Cell Resistance to Chimeric Antigen Receptor T-cell Therapy in Pancreatic Cancer

Kimberly R. Hagel[1,2], Rand Arafeh[1,2], Sydney Gang[1], Taylor E. Arnoff[1], Rebecca C. Larson[3], John G. Doench[2], Nathan D. Mathewson[1,2], Kai W. Wucherpfennig[1,2], Marcela V. Maus[3], and William C. Hahn[1,2,4]

ABSTRACT

Chimeric antigen receptor (CAR) T-cell therapy can lead to dramatic clinical responses in B-cell malignancies. However, early clinical trials with CAR T-cell therapy in non–B-cell malignancies have been disappointing to date, suggesting that tumor-intrinsic features contribute to resistance. To investigate tumor-intrinsic modes of resistance, we performed genome scale CRISPR-Cas9 screens in mesothelin (MSLN)-expressing pancreatic cancer cells. Co-culture with MSLN-targeting CAR T cells identified both antigen-dependent and antigen-independent modes of resistance. In particular, loss of the majority of the genes involved in the pathway responsible for GPI-anchor biosynthesis and attachment abrogated the ability of CAR T cells to target pancreatic cancer cells, suggesting that disruption of this pathway may permit MSLN CAR T-cell evasion in the clinic. Antigen-independent mediators of CAR T-cell response included members of the death receptor pathway as well as genes that regulate tumor transcriptional responses, including *TFAP4* and *INTS12*. TFAP4-mediated CAR T resistance depended on the NFκB transcription factor p65, indicating that tumor resistance to CAR T-cell therapy likely involves alterations in tumor-intrinsic states. Overall, this study uncovers multiple antigen-dependent and -independent mechanisms of CAR T-cell evasion by pancreatic cancer, paving the way for overcoming resistance in this disease that is notoriously refractory to immunotherapy.

Significance: The identification and validation of key determinants of CAR T-cell response in pancreatic cancer provide insights into the landscape of tumor cell intrinsic resistance mechanisms and into approaches to improve therapeutic efficacy.

Introduction

Chimeric antigen receptor (CAR) T-cell therapy has induced profound and lasting effects in B-cell malignancies, leading to the development of 5 FDA-approved therapeutics to date (1–4). This early success has prompted interest in the application of CAR T-cell therapy for solid tumors, which comprise 90% of adult cancers.

Pancreatic cancer is projected to become the second leading cause of cancer-related death by 2040 and has the lowest relative 5-year survival rate among all cancers (5, 6). Pancreatic ductal adenocarcinoma (PDAC) comprises the majority of these cases (7, 8). Chemotherapy and targeted molecular therapies have thus far failed to produce durable clinical responses, promoting interest in novel immunotherapeutic approaches like CAR T-cell therapy. To date, the majority of CAR T-cell clinical trials in PDAC use CAR constructs targeting Mesothelin (MSLN; refs. 9, 10). MSLN is a glycosylphosphatidylinositol (GPI)-linked membrane protein overexpressed in multiple tumor tissues, including pancreatic, colon, ovarian, breast, lung, and gastric cancers. Because of its low expression in normal mesothelial cells, which are commonly considered dispensable, MSLN is an attractive target for CAR T-cell therapy (11). The function of MSLN in normal mesothelial cells is unknown, as *MSLN* knockout mice lack obvious phenotypes (12).

Despite the success of CAR T-cell therapies in B-cell malignancies and the intense interest in testing them in other cancers, CAR-based therapies have been largely unsuccessful in solid tumors thus far (13, 14). In PDAC, the results of early clinical trials point to intrinsic resistance, and even among solid tumors, PDAC appears particularly refractory to CAR T-cell therapy (15–18). The observed resistance is likely multifactorial, including suboptimal T-cell trafficking into the tumor mass and T-cell dysfunction in immunosuppressive solid tumor microenvironments. In addition, tumor-intrinsic factors such as tumor antigen display, tumor expression of immune inhibitory molecules, and intrinsic cell states may affect sensitivity to immune-mediated killing (19–21).

Many groups are working to improve the CAR therapeutic agent in solid tumors, focusing on strategies that boost T-cell function, trafficking, persistence, and on-tumor targeting (22, 23). To identify mechanisms of tumor resistance to CAR T-cell therapy, we performed genome scale CRISPR-Cas9 screens in PDAC cell lines and identified tumor intrinsic, antigen-dependent and -independent mediators of MSLN CAR T-cell efficacy.

Materials and Methods

Cell culture

Lenti-X 293T cells were ordered from Takara Bio (632180, RRID: CVCL_4401). EGFR CAR and untransduced (UTD) T cells were prepared as previously described (24). Tumor cell lines were obtained

[1]Dana-Farber Cancer Institute and Harvard Medical School, Boston, Massachusetts. [2]Broad Institute of MIT and Harvard, Cambridge, Massachusetts. [3]Cellular Immunotherapy Program, Cancer Center, Massachusetts General Hospital and Harvard Medical School, Boston, Massachusetts. [4]Brigham and Women's Hospital, Boston, Massachusetts.

Corresponding Author: William C. Hahn, 450 Brookline Avenue, D1538; Boston, MA 02215. Phone: 617-632-2641; Fax: 617-632-4005; E-mail: william_hahn@dfci.harvard.edu

Cancer Res 2023;83:613–25

doi: 10.1158/0008-5472.CAN-22-2245

from the Broad Institute. Cell culture conditions were as follows: HupT3 (RRID:CVCL_1299): EMEM; KP4 (RRID:CVCL_1338): DMEM/F12; KP3 (RRID:CVCL_3005): RPMI 1640; MIA PaCa-2 (RRID:CVCL_0428)/Lenti-X 293T: DMEM; PACADD-161 (RRID:CVCL_M466)/188 (RRID:CVCL_M469): Dresden media (50% DMEM, 50% Keratinocyte SFM supplemented with 20 ug/mL BPE and 0.2 ng/mL EGF, 20% FBS); JoPaca-1: IMDM; HPAC1 (RRID:CVCL_3517): DMEM/F12 supplemented with insulin (10 mg/mL), transferrin (10 mg/mL), hydrocortisone (50 μg/mL), and EGF (100 μg/mL); Primary human T cells and SupT1 (RRID:CVCL_1714): R10 (RPMI-1640 + Glutamax and Hepes). All media were supplemented with 10% FBS and 1% penicillin–streptomycin, and all cancer cell lines constitutively express Cas9. Tumor cell lines were tested for *Mycoplasma* using PCR (forward primer GGGAGCAAACAGGATTAGATACCCT, reverse primer TGCACCATCTGTCACTCTGTTAACCTC) in May, 2021 and found to be negative. Tumor cell lines were passaged at least one time post thaw before use in any experiment.

Cloning and tumor cell line generation

To generate isogenic stable knockout cell lines, we ligated guide oligos into the pXPR_BRD003 backbone. Briefly, backbone was digested with FastDigest Esp3I (Thermo Fisher Scientific, FERFD0454) and gel purified. Guide oligos were phosphorylated, annealed, and diluted 1:200. Diluted oligos were ligated into the purified backbone using Quick Ligase (VWR, 101227–654). To concurrently knockout 2 genes, we used the pWRS vector gifted by the Sellers laboratory and followed a similar procedure as above, using a single oligo encoding both guides digested out of a cloning vector. To generate cells constitutively expressing Cas9, luciferase, or eGFP/hcRED/TFAP4/MSLN, we used pLX311-Cas9 (RRID:Addgene_118018), pLX313-Firefly luciferase (RRID:Addgene_118017), and pLX-317 encoding each ORF, respectively. To make virus, Lenti-X 293T cells were transfected with the desired construct using third-generation lentiviral packaging vectors pRSV-Rev (RRID:Addgene_12253), pMDLg/pRRE (RRID:Addgene_12251), and pMD2.G (RRID:Addgene_12259) and Lipofectamine 3000 (Thermo Fisher Scientific, L3000015) in Opti-MEM (Thermo Fisher Scientific, 31985088). Virus was collected and pooled 24 and 48 hours post-transfection. For infection, tumor cells were suspended in media supplemented with Polybrene (8 μg/mL, Santa Cruz Biotechnology, SC-134220), plated with dropwise addition of lentivirus, and centrifuged (2,000 RPM, 30°C, 2 hours). Guide sequences listed in Supplementary Table S5.

MSLN CAR cloning and virus

The MSLN CAR sequence, encoding SS1 ScFv, CD8 hinge, CD28 transmembrane and signaling domains, and CD3 zeta chain, was designed and shared by the Wucherpfennig laboratory. This sequence, followed by a P2A-mCherry element, was cloned into the pTRPe lentiviral expression backbone, gifted by the June laboratory. Pooled virus was concentrated approximately 300 × *g* via ultra-centrifugation (25,000 RPM, 4°C, 2 hours). Titer was determined by serial dilution and infection of SupT1 cells followed by flow cytometry to quantify the percentage of mCherry-positive cells.

MSLN CAR T-cell generation

Blood from healthy donors was obtained from apheresis leukoreduction collars (Brigham and Women's Hospital, Crimson Core). Peripheral blood mononuclear cells were extracted using centrifugation (35 minutes, 400 × *g*) through Ficoll Paque (Sigma-Aldrich, GE17–1440–02). T cells were isolated using the EasySep Human T-cell Isolation Kit (StemCell Technologies, 17951) and the Big Easy magnet (StemCell, 18001), according to the manufacturer's protocol. T cells were stimulated with CD3/CD28-coated Dynabeads (Thermo Fisher Scientific, 11131D) and maintained in R10 supplemented with 20 U/mL IL2. 24–30 hours after isolation, T cells were infected with MSLN CAR by adding lentivirus dropwise to each well at an MOI of 5–6; infection efficiencies ranged from approximately 50% to 75%. 7 days after isolation, Dynabeads were removed; 14 days after isolation, T cells were frozen in 90% FBS supplemented with 10% DMSO. Fifteen to 20 hours before plating a coculture, T cells were thawed and cultured in R10 sans IL2.

CRISPR-Cas9 screens

HupT3 and KP4_MSLN cells were infected with the Brunello lentiviral library (Genetics Perturbation Platform, Broad Institute). The HupT3 screen was performed in biological triplicate and the KP4 screen was performed in biological duplicate, with each replicate using T cells from a different donor. The library virus was titered to achieve an MOI less than 1; the infection efficiencies are as follows: HupT3: Rep 1, 19.6% infection; Rep 2, 26.3% infection; Rep 3, 31.1% infection; KP4_MSLN: Rep 1, 20.3% infection; Rep 2, 18.5% infection. 24 hours after infection, cells were split into puromycin (HupT3: 1.5 μg/mL, 9–13 days; KP4_MSLN: 2 μg/mL, 6–7 days). Following selection, cells were plated in cocultures with MSLN CAR or UTD cells (HupT3: 14–15 days after infection, 48 hours coculture, E:T of 2:1 or 4:1, depending on T-cell donor; KP4_MSLN: 10 days after infection, 72 hours coculture, E:T of 1:1). Cell pellets were collected at each passage and post coculture. DNA was extracted from small pellets (<5e6 cells) using NucleoSpin Blood Mini Kits (Machery-Nagel 740951.50) and from large pellets (up to 1e8) using QIAamp DNA Blood Maxi Kits (Qiagen 51192). Barcodes were PCR amplified and Illumina sequenced. The z-score of the difference between $\log_2$ normalized guide counts in CAR cocultures versus UTD cocultures were used as inputs for hypergeometric analyses to calculate final ranked scores for each gene.

RNA sequencing

RNA was collected in triplicate from HupT3 cells using RNeasy Plus Mini Kit (Qiagen 74134). RNA sequencing (RNA-seq) was performed by the Molecular Biology Core Facilities at Dana-Farber Cancer Institute using KAPA mRNA HyperPrep Kits. Briefly, mRNA transcripts were enriched using oligo-dT beads, fragmented, and reverse transcribed into cDNA via random priming. Following addition of Illumina adapters, cDNA transcripts were amplified and sequenced. Transcript reads were aligned via STAR; downstream processing was achieved using Cufflinks and DESeq (RRID:SCR_000154).

Animal studies

All studies were performed in 5–6-week-old female NSG mice (RRID:IMSR_JAX:005557) and were approved under Institutional Animal Care and Use Committee protocol 04–101. For the GPAA1 knockdown experiment, PACADD-161 PDAC cells were infected with control guide IGC.2 or GPAA1.1, selected in puromycin (1.5 μg/mL) for 72 hours, and injected subcutaneously with Matrigel (1:1 ratio, Corning, 356231) into the flanks of NSG mice after a 48-hour period to recover from selection ($n = 14$ per group). When the average tumor volume reached approximately 100 mm^3, a single dose of 5e6 T cells (MSLN CAR or UTD) was administered via tail vein. Tumor volume was monitored via caliper measurement every 3 to 4 days. For the TFAP4 overexpression experiment, we performed the same steps as above, with the following changes: $n = 12$ mice per group; average tumor volume at time of treatment = approximately 150 mm^3; T cells

injected = 2e6. Mice were sacrificed when tumors reached a volume of approximately 1,200 mm^3 or became necrotic. In all cases, mice were randomly distributed to treatment groups using caliper measurements to achieve comparable average tumor size between groups.

Cocultures

Coculture conditions vary depending on the T-cell donor, the tumor cell type, and the plate format. Briefly, T cells were plated concurrently with tumor cells to achieve the desired E:T ratio, using equal parts T-cell and tumor cell media. Cocultures are allowed to proceed for 24–72 hours. Surviving target cells were quantified using either flow cytometry or luciferase assay; in both cases, survival was calculated by taking the ratio of a population's value (cell number or luciferase signal, respectively) in CAR T-cell cocultures versus UTD T-cell cocultures.

Flow cytometry

Unless otherwise stated, all washes and staining were done using FACS wash (1X PBS + 5% FBS) and all analyses were performed on BD LSR Fortessa cytometers. For post coculture target cell enumeration, media were aspirated, and cultures were washed with PBS to remove most dead target cells and suspended T cells. Remaining cells were then detached, washed, and stained for CD45 or CD2 to mark residual T cells and Ep-CAM to mark surviving tumor cells (3:100, 20 minutes, 4°C). Samples were fixed with 4% paraformaldehyde in PBS (BioLegend 420801, 15 minutes, room temperature), spiked with CountBright Absolute Counting Beads (Thermo Fisher Scientific, C36950, 30/200 μL sample), and analyzed. PDAC populations ($CD45/CD2^{low}$, $Ep\text{-}CAM^{high}$) were gated, and bead counts were used to quantify cell number according to the manufacturer's protocol. To stain for MSLN surface expression, cells were incubated at room temperature for 30 minutes with primary antibody. To stain T cells for activation markers, cells were stained with Zombie violet (BioLegend 423113, 20 minutes, room temperature) and CD25/CD69 (20 minutes, 4°C), fixed and permeabilized (eBiosciences, 00–5223–56), stained with intracellular markers IFNγ/Ki67 (20 minutes, room temperature), and resuspended in FACS wash before analysis. To stain for FASL surface expression, coculture supernatants were collected, stained with Zombie NIR (BioLegend, 423106, 20 minutes, room temperature), stained with PE-CD2, AF647-Ep-CAM, and BV421-FASL (20 minutes, 4°C), and fixed with 4% paraformaldehyde in PBS (BioLegend 420801, 15 minutes, room temperature). Antibodies are listed in Supplementary Table S5.

Luciferase assay

ONE-Glo EX Luciferase Assays (Promega, E8120) were used to quantify 96-well cocultures of T cells with target cells constitutively expressing firefly luciferase according to the manufacturer's protocol. 70 μL of room temperature diluted ONE-Glo EX luciferase substrate was added per well. Plates were read on a PerkinElmer Envision at least 3 minutes after substrate addition.

qRT-PCR

RNA was isolated using RNeasy Plus Mini Kit (Qiagen 74134). 1 μg/sample was reverse transcribed into cDNA using SuperScript VILO Master Mix (Thermo Fisher Scientific, 11755050) according to the manufacturer's protocol. cDNA products were diluted 1:50 in Ultra-Pure water (Thermo Fisher Scientific, 10977023), and combined with primers (1 μmol/L) and Power CYBR Green PCR Master Mix (Thermo Fisher Scientific, 4368708). Relative gene expression changes were calculated using the delta-delta-C_t method and normalized using amplification of the RPLP0 housekeeping gene. Primers listed in Supplementary Table S5.

Immunoblots

Cells were lysed using 1X RIPA Buffer (END Millipore, 20–188) with Pierce protease inhibitors (Thermo Fisher Scientific, A32953). Protein concentration was quantified using BCA assay (Thermo Fisher Scientific, PI23225). 30/20 μL protein was loaded onto NuPAGE Bis Tris Gels (Thermo Fisher Scientific) and, with the exception of SMARCA4 blots, transferred onto PVDF or nitrocellulose using the iBlot2 (Thermo Fisher Scientific) and blocked in Intercept Blocking Buffer (LI-COR, 927–70010). To blot for SMARCA4, a wet transfer was performed (200 mA, 2 hours, on ice) using 1X NuPAGE transfer buffer (NP00061) supplemented with 20% methanol. Membranes were then blocked in 5% non-fat milk. All membranes were stained in primary antibody (overnight, 4°C), washed 3X in PBST, stained in LI-COR IRDye 680/800 (Thermo Fisher Scientific, 30 minutes, room temperature), washed 3x in PBST, and imaged on the LI-COR Odyssey. Images were processed using Fiji by ImageJ (RRID: SCR_002285). Antibodies listed in Supplementary Table S5.

ELISA

MSLN CAR or UTD T cells were cultured in triplicate in the presence or absence of HupT3 cells for activation. Undiluted supernatants were collected at 24 hours and the TNFα concentration was quantified via ELISA (Abcam, ab-181421) following the manufacturer's protocol.

Statistical analysis

Significance in all coculture experiments was calculated by comparing the indicated gene knockdown or overexpression with the control knockdown or overexpression; in experiments with two controls, significance was calculated relative to the first control shown. Throughout, the Dunnett multiple comparisons test was performed to compare multiple experimental conditions with a single control; multiple unpaired *t* tests were performed to compare single experimental conditions with a corresponding control.

Data availability

The data presented in this study are provided in the main article and Supplementary Materials. RNA-seq data have also been deposited in NCBI's Gene Expression Omnibus (series accession number GSE220614; ref. 25).

Results

Identifying mediators of MSLN CAR T-cell resistance and sensitivity using genome scale CRISPR-Cas9 loss-of-function screens

To generate a CAR T-cell specific for MSLN, we used a second-generation CAR construct comprising the SS1 single-chain variable fragment paired with the CD28 costimulatory domain. We confirmed the antigen specificity of our MSLN CAR construct by performing coculture experiments with PDAC cell lines displaying different levels of endogenous MSLN. Specifically, we found that the MSLN CAR T cells killed the $MSLN^+$ lines in a dose-dependent manner yet failed to kill $MSLN^-$ lines (Supplementary Fig. S1A). To interrogate the capacity of this CAR construct to discern Cas9-mediated perturbations of MSLN, we performed cocultures with HupT3 cells, which endogenously express MSLN at a moderate level, or KP4_MSLN cells, which ectopically overexpress MSLN, following knockout of *MSLN* or an intergenic control locus (**Fig. 1A**). In both cases, loss of MSLN

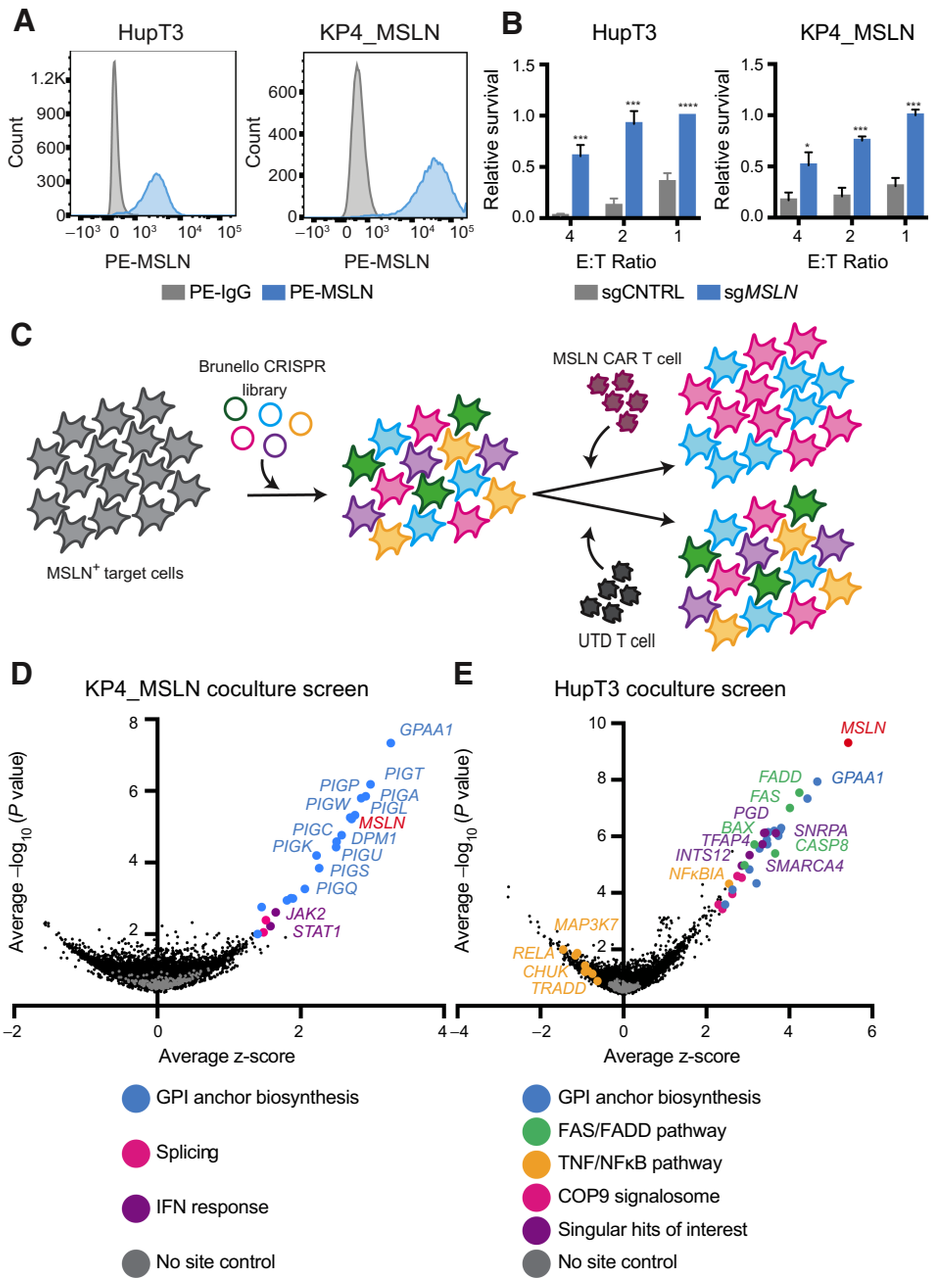

Figure 1.
Genome scale CRISPR-Cas9 screens in PDAC. **A,** Endogenous MSLN expression in HupT3 cells and the exogenous MSLN expression in KP4_MSLN cells. **B,** HupT3/KP4_MSLN cell number, quantified by FACS, following knockout of luciferase (sgCNTRL) or MSLN and coculture with MSLN CAR T or UTD cells at the indicated E:T ratios for 48 hours ($n = 3$, t test). **C,** Schematic of HupT3 and KP4_MSLN coculture screens, performed in biological triplicate and duplicate, respectively. **D** and **E,** Gene level guide scores displayed as average $-\log_{10}(P \text{ value})$ versus average z-score, calculated by hypergeometric distribution. *, $P < 0.05$; ***, $P < 0.001$; ****, $P < 0.0001$.

abrogated the ability of these CAR T cells to kill PDAC cells (**Fig. 1B**; Supplementary Fig. S1B).

To supplement these findings, we assessed the immunologic response of CAR T cells to stimulation. Specifically, after coculture with MSLN-expressing KP4 PDAC cells, we found that MSLN CAR T cells exhibited increased expression of the activation markers CD25 and CD69, produced higher levels of IFNγ, and showed increased proliferation, as assessed by Ki67 staining (Supplementary Fig. S1C). Coculture with luciferase-expressing KP4 cells failed to elicit the same response. Taken together, these observations confirmed that expression of this particular CAR conferred specificity for MSLN.

Using this MLSN CAR construct to apply immunological pressure, we systematically interrogated genes that affect tumor cell sensitivity to CAR killing. To do so, we used the Brunello CRISPR-Cas9 library in HupT3 and KP4_MSLN cells followed by coculture with MLSN CAR or donor-matched UTD T cells (**Fig. 1C**; Supplementary Table S1; ref. 26).

In the KP4 cells that express ectopic MSLN, we found that genes related to the regulation of MSLN expression were significantly enriched in the screen, with significance being defined using a P value less than 0.05 (**Fig. 1D**; Supplementary Fig. S1D). Specifically, with the exception of MSLN itself, the top 16 candidates are all involved in the biosynthesis and attachment of the GPI anchor to nascent proteins in the endoplasmic reticulum (ER). Beginning in the cytoplasm and ending in the ER lumen, the Phosphatidyl Inositol Glycan (PIG) proteins sequentially construct a core glycan comprised of mannose,

glucosamine, and inositol that is capped on one end by a membrane-anchoring phospholipid tail and on the other end by a phosphoethanolamine (PEtN) moiety. Once constructed, the transamidase complex, consisting of PIGK, GPAA1, PIGU, PIGT, and PIGS, transfers the GPI anchor into the C-terminus of the nascent protein via the PEtN linker. Because MSLN is a GPI-anchored membrane protein, deficiencies in GPI anchor biosynthesis would be expected to reduce MSLN expression. These observations indicate that, in cells that ectopically express high levels of MSLN, antigen expression is the major determinant of MSLN-directed CAR T-cell responses.

In HupT3 cells that endogenously express MSLN, we also found a prominent enrichment in members of the GPI-anchor pathway. In addition, we found many other putative regulators of CAR T-cell sensitivity (**Fig. 1E**; Supplementary Fig. S1E). Among the top-scoring hits, defined by candidates with log *P* values greater than 4, were members of the death receptor pathway *FADD*, *FAS*, *BAX*, *BID*, and *CASP8*. Additional top hits included the endosomal trafficking genes *AP2M1*, *AP2S*1, *DNM2*, splicing factor *SNRPA*, pentose phosphate shunt enzyme *PGD*, and transcriptional regulators *SMARCA4, INTS12*, and *TFAP4*. Furthermore, although the screening conditions were optimized to identify sgRNAs that enhanced tumor cell survival, we noted that multiple sgRNAs targeting the NFκB regulatory network were depleted in the screen, suggesting strong negative selection to maintain the activity of this pathway.

In comparing both screens, we noted a correlation between highly enriched genes (Supplementary Fig. S1F). Furthermore, in keeping with previous studies, we noted enrichment in IFNγ pathway members in both screens (Supplementary Fig. S1G; refs. 20, 27, 28). While scoring less strongly than the GPI anchor biosynthesis genes, multiple IFNγ-related genes were significantly enriched in the KP4 screen, including *STAT1*, *JAK2*, and *IFNGR2*. In the HupT3 screen, IFNγ pathway members were more modestly enriched, indicating that alternative signaling axes may play a more prominent role in CAR T-cell sensitization in this context.

Deficiencies in GPI anchor machinery confer MSLN CAR T resistance

Because the GPI anchor biosynthesis pathway scored strongly in both the HupT3 and KP4 screens, we validated these findings by knocking out GPAA1, a member of the transamidase complex responsible for transferring the GPI anchor onto the C-terminus of nascent proteins. We confirmed that KO of *GPAA1* in HupT3 cells induced loss of MSLN surface expression and conferred resistance to MSLN CAR T cells at multiple effector: target (E:T) ratios, validating *GPAA1* as a strong antigen-dependent hit (**Fig. 2A**). To validate the relevance of this pathway more thoroughly, we knocked out two additional members, *PIGA* and *PIGW*, in both HupT3 and KP4_MSLN cells (Supplementary Fig. S2A). Loss of each pathway member caused MSLN CAR T resistance in the coculture setting and loss of MSLN expression at the cell surface (**Fig. 2B** and **C**).

To investigate the relevance of this finding *in vivo*, we knocked out *GPAA1* in PACADD-161 PDAC cells and injected them subcutaneously into the flanks of NSG mice (Supplementary Fig. S2B). Compared with control tumors, *GPAA1* KO tumors were less sensitive to MSLN CAR T-cell therapy (**Fig. 2D**). Deletion of *GPAA1, PIGA*, and *PIGW* did not have a pronounced effect on viability in either PDAC cell line; this observation is concordant with analyses of the Cancer Dependency Map, a dataset composed of genome scale loss-of-function fitness screens performed in hundreds of human cancer cell lines, which indicate that members of the GPI biosynthesis pathway are not strong dependencies in pancreatic cancer (Supplementary Fig. S2C; refs. 29, 30). Together, these observations suggest that alteration of the GPI anchor biosynthesis and transfer machinery confers resistance to MSLN CAR T cells and, due to the absence of dependency on many pathway members, disruption of this machinery may emerge as a prominent mode of clinical resistance to MSLN CAR T-cell therapy.

Polarization of the death receptor pathways affect CAR T-cell killing

Next, we focused on candidates outside of the GPI anchor pathway, beginning with the death receptor family. Notably, *FAS, FADD*, and multiple downstream signaling partners scored strongly in the HupT3 screen, indicating that this pathway normally serves to sensitize PDAC cells to MSLN CAR killing (**Fig. 3A** and **B**). In contrast, multiple components downstream of the TNFR1 death receptor were depleted in the screen. Cells harboring sgRNA targeting the NFκB transcription factor *RELA* (p65) in particular were preferentially depleted in the presence of MSLN CAR T cells. The same was true of cells lacking *CHUK* (IKKA), a component of the IKK complex that activates NFκB by phosphorylating members of the IκB family, and *MAP3K7* (TAK1), which activates IKK. sgRNAs targeting *NFKBIA*, encoding the IκBα protein that negatively regulates this pathway by sequestering NFκB dimers in the cytoplasm, were highly enriched in the screen (**Fig. 3A** and **B**).

To directly test the importance of these divergent death receptor pathways, we cocultured *FADD* or *RELA* knockout HupT3 cells with MSLN CAR T cells. Although loss of FADD conferred marked resistance to CAR T-cell killing, loss of p65 induced significant sensitivity to CAR T-cell killing (**Fig. 3C**; Supplementary Fig. S3B). Loss of p65 also sensitized additional PDAC lines to CAR T-cell killing (Supplementary Fig. S3A). Notably, loss of *NFκB2* (p52) failed to sensitize HupT3 cells to CAR T-mediated death, indicating that the observed sensitization was specific for *RELA* (**Fig. 3D**; Supplementary Fig. S3B). In contrast, activation of p65 by knockout of *NFκBIA* (IκBα) induced the opposite effect, conferring protection in MSLN CAR T-cell cocultures (**Fig. 3C**; Supplementary Fig. S3B).

To interrogate the role of CAR T cells in death receptor pathway activation, we cultured MSLN CAR and UTD T cells ± HupT3 cells and found that MSLN CAR T cells express both FASL and TNFα upon activation with antigen-expressing tumor cells (**Fig. 3E**). Furthermore, coculture experiments with neutralizing antibodies showed that neutralization of FAS promotes tumor cell evasion of T-cell killing, whereas neutralization of TNFα promotes tumor susceptibility to T-cell killing (**Fig. 3F**). Together, these observations suggest that, at baseline, the FAS/FADD pathway contributes to CAR T-cell killing while the TNF/NFκB pathway promotes CAR T-cell evasion in PDAC cells.

TFAP4 modulates CAR sensitivity in epithelial tumors

We then focused on the candidates that were previously unknown to mediate CAR T sensitivity. We used STRING analyses to identify enriched pathways and complexes from the HupT3 screen (31). We then nominated representative members of these pathways and complexes, as well as solitary top-scoring hits, for individual validation. Specifically, we knocked out 8 candidate genes in HupT3 cells and performed coculture time courses with MSLN CAR T cells at multiple E:T ratios; of these, 5 candidates validated strongly, as their knockout conferred significant survival advantages in MSLN CAR T cocultures under multiple conditions (**Fig. 4A**; Supplementary Fig. S4A and S4C).

To determine whether these genes were conferring antigen-dependent or -independent resistance, we used flow cytometry to

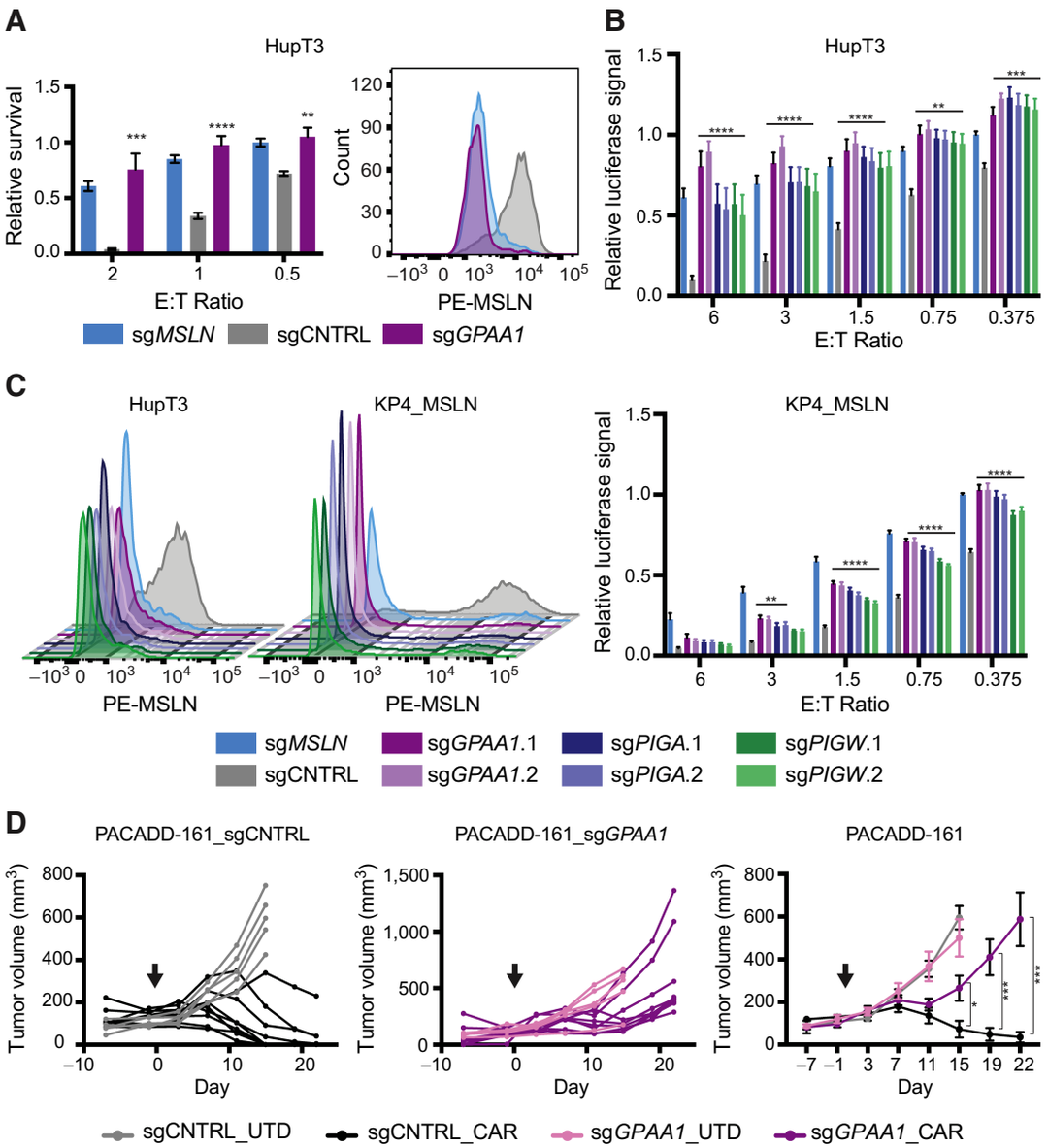

Figure 2.

Validation of the GPI anchor biosynthesis pathway. **A,** HupT3 cell number, quantified by FACS, following knockout of intergenic control locus or MSLN and coculture with MSLN CAR T or UTD cells at the indicated E:T ratios for 48 hours ($n = 3$; t test); FACS plot showing the impact of GPAA1 loss on MSLN. **B,** HupT3/KP4_MSLN cell survival, quantified by firefly luciferase assay, following knockout of intergenic control locus, *MSLN, GPAA1, PIGA*, or *PIGW* and coculture with MSLN CAR T or UTD cells at the indicated E:T ratios (HupT3: 24 hours, $n = 3$; KP4_MSLN: 72 hours, $n = 3$; Dunnett test). **C,** FACS plots showing the impact of GPAA1, PIGA, or PIGW loss on MSLN expression. **D,** Volume of tumors formed by PACADD-161 cells infected with control ($n = 10$) or GPAA1 ($n = 18$) guides and injected into the flanks of NSG mice; 5M CAR or UTD cells injected intravenously at day 0 (t test; arrow, T-cell injection). *, $P < 0.05$; **, $P < 0.01$; ***, $P < 0.001$; ****, $P < 0.0001$.

assess the impact of knocking out each hit on surface MSLN expression (**Fig. 4B**; Supplementary Fig. S4B). The splicing factor SNRPA exhibited the most profound effect on antigen expression, causing a marked reduction in MSLN at the cell surface; loss of SMARCA4, a catalytic component of the mSWI/SNF complex, also induced a modest but consistent downward shift in MSLN expression. Knockout of PGD, a member of the pentose phosphate shunt, induced a slight and inconsistent reduction in MSLN expression that did not correlate with evasion of MSLN CAR T-cell killing. In addition, knockout of endosomal-trafficking protein AP2M1 also caused a marked loss of MSLN expression and some resistance to MSLN CAR T-cell killing (Supplementary Fig. S4D). Finally, loss of INTS12 and TFAP4 did not affect MSLN expression at the cell surface, indicating that their impact on MSLN CAR T-cell sensitivity is antigen independent.

To explore the mechanisms underlying CAR T-cell resistance, we focused on the antigen-agnostic hits, anticipating that these candidates

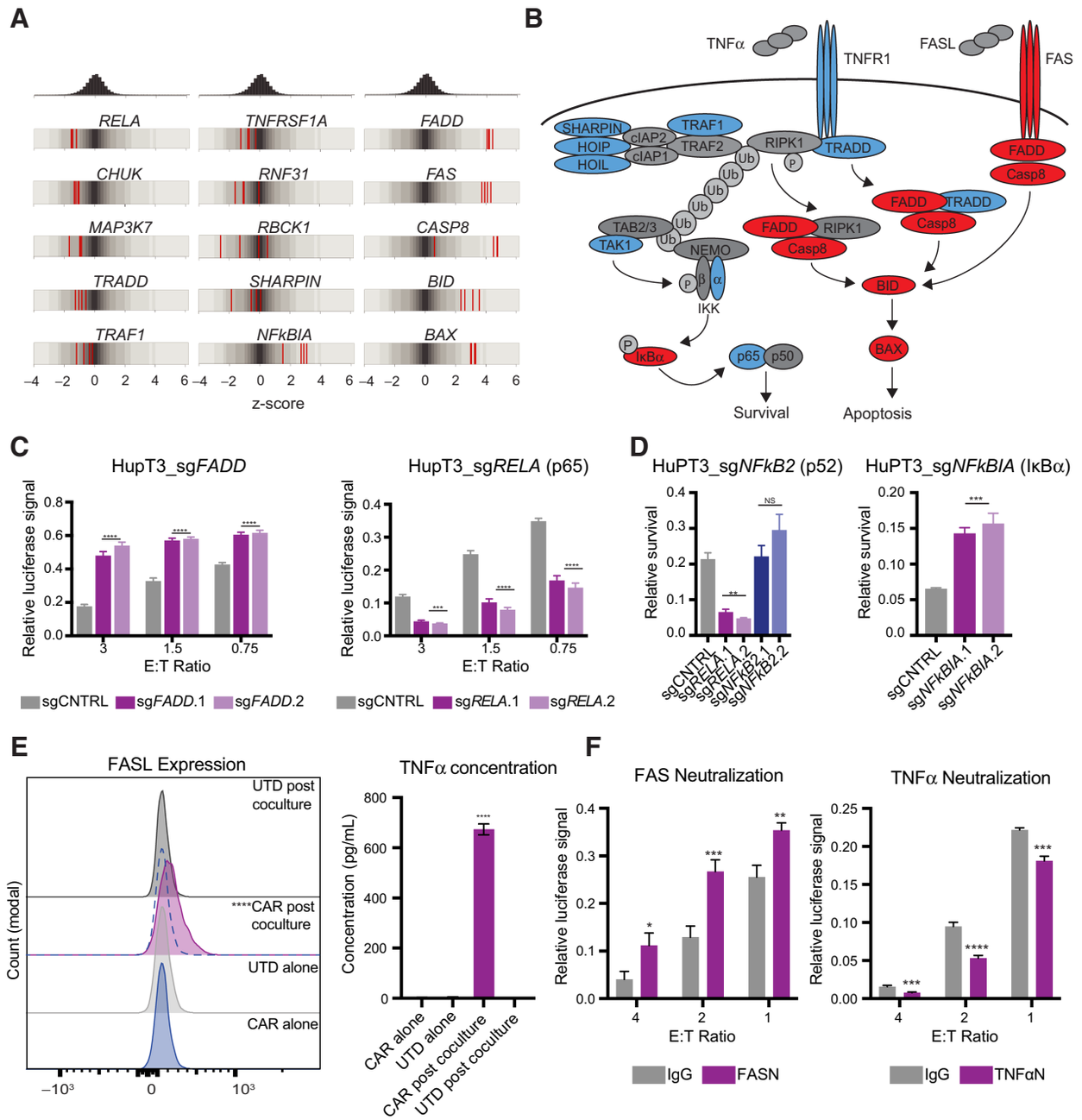

Figure 3.

Polarization of the death receptor pathways in CAR T-cell sensitivity. **A,** Histograms and heatmaps showing the distribution of guide scores in the HupT3 screen, quantified by taking the Z-score of the difference between $\log_2$ normalized guide read counts in the MSLN CAR T cells and UTD coculture screen arms. Red lines, the four guides targeting the indicated gene. **B,** Graphical depiction of the FAS and TNFR1 death receptor pathways. Red, corresponding gene was enriched in the HupT3 screen; blue, corresponding gene was depleted in the HupT3 screen (genes were considered enriched if their z-score exceeded 4 and depleted if their z-score exceeded −0.5). **C,** Survival of HupT3 cells, quantified by firefly luciferase assay, upon knockout of an intergenic control locus, *FADD*, or *RELA* and coculture with MSLN CAR T or UTD control cells for 24 hours ($n = 3$; Dunnett test). **D,** HupT3 cell number, quantified by FACS, upon knockout of intergenic control, *RELA*, *NFκB2*, or *NFκBIA* and coculture with MSLN CAR T or UTD control cells for 48 hours (*sgRELA/NFκB2*: $n = 3$, E:T at 1–1.5, depending on T-cell donor; sg*NFκBIA*: $n = 3$, E:T at 2; Dunnett test). **E,** FASL expression and TNFα concentration, quantified by FACS and ELISA, respectively, of the indicated T-cell populations after 24 hours of culture ± HupT3 cells ($n = 3$, *t* test, CAR post coculture vs. CAR alone). In FACS plot, dashed purple line represents the FASL expression of CARs cultured alone; *t* test was performed using the median fluorescence intensity of each population in triplicate. **F,** HupT3 survival following 24 hours coculture with MSLN CAR T or UTD cells ± FAS (1,000 ng/mL) or TNFα (250 ng/mL) neutralizing antibody, or the corresponding IgG control antibodies. *, $P < 0.05$; **, $P < 0.01$; ***, $P < 0.001$; ****, $P < 0.0001$; NS, not significant.

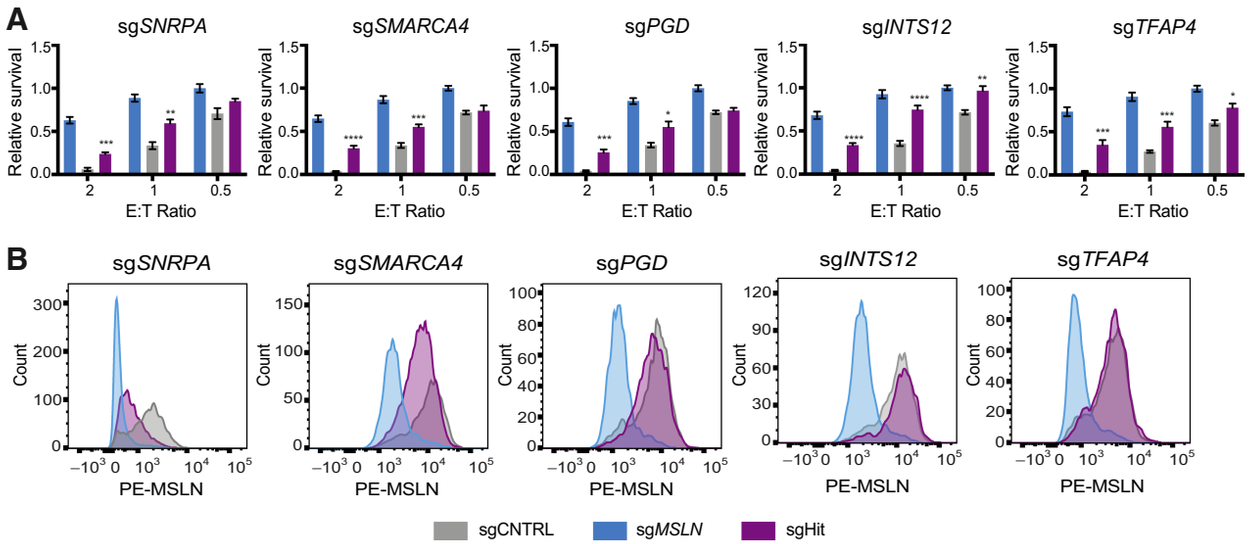

Figure 4.

HupT3 coculture screen validation. **A,** HupT3 cell number, quantified by FACS, following knockout of intergenic control locus, *SNPRA* ($n = 3$), *SMARCA4* ($n = 3$), *PGD* ($n = 3$), *INTS12* ($n = 3$), or *TFAP4* ($n = 4$) and cocultured with MSLN CAR or UTD T cells at the indicated E:T ratios for 48 hours (*t* test). **B,** FACS plots showing the impact of each knockout on MSLN expression. *, $P < 0.05$; **, $P < 0.01$; ***, $P < 0.001$; ****, $P < 0.0001$.

may be important for all CAR T-cell therapies. Of these, TFAP4 was of particular interest due to its strong validation and broad impact in multiple PDAC cell lines. Specifically, to explore the effect of TFAP4 loss outside of the HupT3 cell line, we showed that TFAP4 loss in 5 additional pancreatic cancer cell lines conferred significant resistance to killing by MSLN CAR T cells (**Fig. 5A**; Supplementary Fig. S5A). In contrast, forced overexpression of TFAP4 elicited the opposite phenotype, with TFAP4-overexpressing PDAC lines showing increased sensitivity to MSLN CAR T-cell killing (**Fig. 5B**; Supplementary Fig. S5B). This finding extended outside of PDAC, as modulation of TFAP4 also sensitize $MSLN^{+}$ colon and ovarian cells to MSLN CAR T-cell killing (Supplementary Fig. S5A–S5D). To probe the antigen-agnostic aspects of TFAP4-mediated CAR sensitivity, we cocultured PDAC cells with CAR T cells targeting EGFR. As with the MSLN CAR T cocultures, TFAP4 loss reduced sensitivity to CAR killing, whereas TFAP4 overexpression increased sensitivity to CAR killing (**Fig. 5C**; Supplementary Fig. S5E).

In addition, although outside of our initial validation efforts, we noted that *MYC* also scored strongly in the HupT3 screen. Because TFAP4 is a well validated direct target of MYC, we hypothesized that the enrichment of *MYC* knockout cells in our screen may have been the result of a reduction in TFAP4 expression (32). Indeed, we validated MYC as a modulator of CAR T-cell sensitivity, showing that MYC knockout in HupT3 cells leads to enhanced survival upon MSLN CAR T coculture; as with TFAP4, this survival advantage was independent of changes in MSLN expression (Supplementary Fig. S5F). Furthermore, we confirmed that MYC depletion resulted in reduced TFAP4 protein levels, supporting the idea that MYC loss may confer CAR T-cell sensitivity through modulations of TFAP4 (Supplementary Fig. S5G). In sum, the enrichment and validation of both TFAP4 and MYC reinforced the evidence supporting this transcriptional program in CAR T-cell sensitivity.

To assess the impact of TFAP4 on the efficacy of MSLN CAR T-cell therapy in an *in vivo* setting, we injected 1.5 million TFAP4 or eGFP overexpressing PACADD-161 cells into the flanks of NSG mice. When the average tumor volume reached approximately 150 mm^3, we intravenously injected a single dose of 2 million T cells (either MSLN CAR or UTD). Although the majority of eGFP tumors showed progression despite therapy, the majority of TFAP4 tumors showed partial or complete responses (**Fig. 5D**). These observations confirmed that increasing the expression of TFAP4 further sensitized PDAC cells to MSLN CAR T-cell therapy and identified TFAP4 as a major antigen-independent regulator of tumor sensitivity to CAR T-cell therapy.

TFAP4 modulates p65 activity

To interrogate the mechanism of TFAP4-mediated CAR T-cell sensitivity, we analyzed the consequences of manipulating TFAP4 on gene expression. Because TFAP4 loss and gain induced opposite phenotypes in CAR T-cell coculture, we performed RNA-seq following knockout and overexpression of TFAP4 in HupT3 cells to capture transcripts that changed in diametric directions (**Fig. 6A** and **B**). Indeed, we found strong differential gene expression contingent upon TFAP4 expression (**Fig. 6B**; Supplementary Table S2). Using this dataset, we performed GSEA and found that IFN signatures were notably enriched following TFAP4 knockout and decreased upon TFAP4 overexpression (**Fig. 6C**; Supplementary Table S3).

We confirmed these findings by measuring the expression of IFN-stimulated genes (ISG) by qRT-PCR following TFAP4 loss, in combination with either MSLN CAR T coculture or IFNγ treatment to enhance ISG transcription, in HupT3 cells (Supplementary Fig. S6A; Supplementary Table S5). We found that TFAP4 loss alone induced increased expression of multiple ISGs. In addition, treatment with IFNγ or coculture with MSLN CAR T cells augmented induction of select ISGs in TFAP4 knockout cells. These observations suggested that the loss of TFAP4 primes cells to respond to external stimuli such as IFNs, generating a sustained IFN-responsive cell state. Because sustained IFN signaling has been shown to confer resistance to T-cell killing, we also tested the impact of pre-conditioning HupT3 cells in type I/II IFNs (33). After sustained (>7 days) culture and passage in the presence of 100 ng/mL

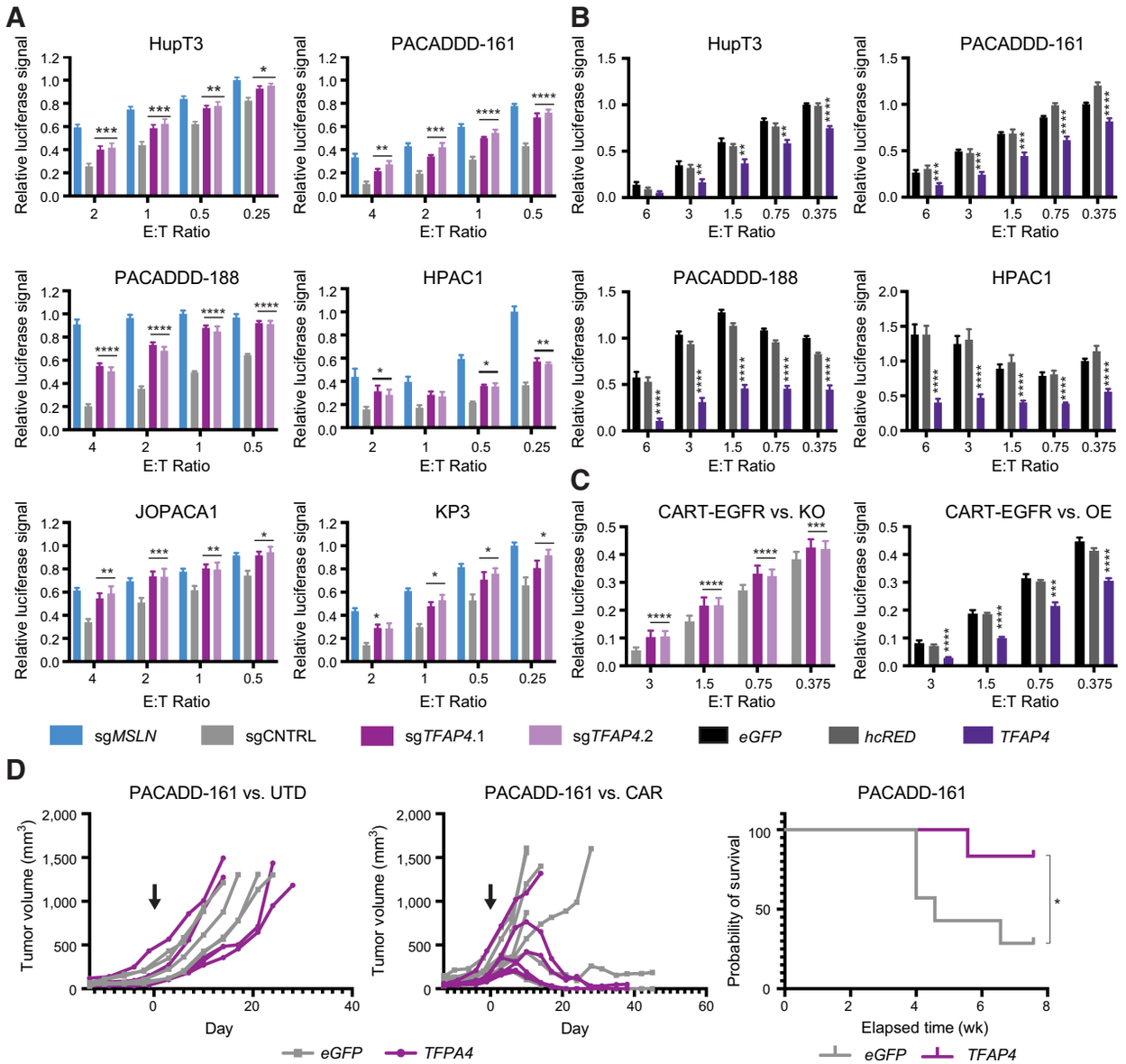

Figure 5.

TFAP4 as a mediator of CAR T-cell sensitivity. **A,** Survival of the indicated PDAC cell lines, quantified by firefly luciferase assay, following knockout of an intergenic control locus or TFAP4 and coculture with MSLN CAR T or UTD cells at the indicated E:T ratios (HupT3: 24 hours coculture, $n = 4$; PACADD-161: 48 hours coculture, $n = 3$; PACADD-188: 72 hours coculture, $n = 3$; KP3: 72 hours coculture, $n = 4$; HPAC: 72 hours cocultures, $n = 3$; JoPaca-1: 48 hours cocultures, $n = 3$; Dunnett test). **B,** Survival of the indicated PDAC cell lines, quantified by firefly luciferase assay, following the overexpression of eGFP, hcRED, or TFAP4 and coculture with MSLN CAR T or UTD cells at the indicated E:T ratios (HupT3: 24 hours coculture, $n = 4$; PACADD-161: 48 hours coculture, $n = 3$; PACADD-188: 72 hours coculture, $n = 3$; HPAC: 72 hours cocultures, $n = 3$; t test). **C,** Survival of HupT3 cells following knockout or overexpression of TFAP4 and coculture with EGFR CAR T or UTD cells at the indicated E:T ratios for 24 hours (KO: $n = 5$, Dunnett test; OE: $n = 3$, t test). **D,** Volume of PACADD-161 tumors overexpressing eGFP ($n = 12$) or TFAP4 ($n = 11$) following injection into the flanks of NSG mice; 2M CAR or UTD cells intravenously injected at day 0 (arrow, T-cell injection; log-rank test); Kaplan–Meier curve showing the survival of mice harboring EGFP or TFAP4 overexpressing tumors. *, $P < 0.05$; **, $P < 0.01$; ***, $P < 0.001$; ****, $P < 0.0001$.

IFNγ or IFNβ, HupT3 cells cocultured with MSLN CAR T cells showed increased resistance to killing, supporting the hypothesis that persistent upregulation of ISGs affects MSLN CAR T-cell sensitivity (Supplementary Fig. S6B). These data suggest that TFAP4-mediated changes to basal ISG expression could contribute to CAR T-cell sensitivity and resistance.

Because the absence of TFAP4 caused an increase in ISG expression and a CAR T-cell–resistant cell state, we hypothesized that a secondary factor might play a role in mediating both phenotypes. Notably, NFκB is a well-documented mediator of select ISG transcription, and our work showed the importance of this transcription factor in MSLN CAR T-cell evasion (**Fig. 3**; ref. 34). In support of the putative connection between

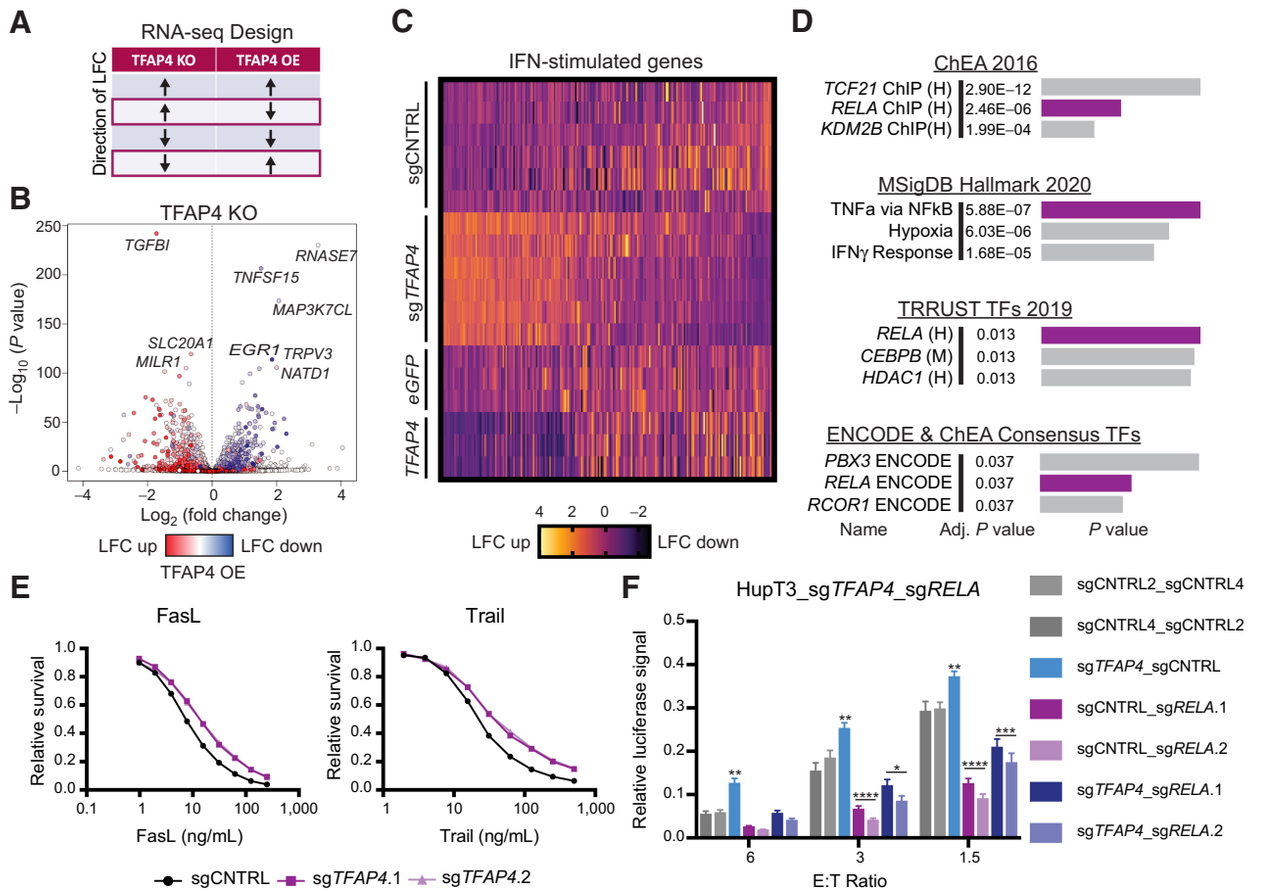

Figure 6.

TFAP4 and NFκB as cooperating mediators of CAR T-cell sensitivity. **A,** Schematic of RNA-seq experimental design; overlap highlights genes of highest interest, with differential transcriptional changes upon TFAP4 loss and gain. **B,** Volcano plot showing differential gene expression upon TFAP4 knockout in HupT3 cells and colored according to the LFC of each gene in TFAP4 overexpressing HupT3 cells. **C,** MSigDB Hallmark gene sets for IFN alpha response (M5911) and IFNγ response (M5913) clustered according to their differential expression in HupT3 cells upon TFAP4 loss and overexpression (z-score of TPM value mapped for each gene); MSigDB gene sets combined to remove duplicates. **D,** Transcriptional and pathway enrichments, identified by Enrichr, of genes upregulated upon TFAP4 knockout with a $\log_2 P$ value of >20 [input of 565 genes; H, human; M, mouse; adjusted *P* value calculated via Benjamini–Hochberg method; bar length corresponds to *P* value (Fisher exact test)]. Purple, *RELA*/NFκB-related enrichments. **E,** Survival curves, quantified by CTG assay, of HupT3 cells following knockout of TFAP4 and treatment with multimeric FASL or TRAIL at the indicated concentrations for 24 hours ($n = 3$ each). **F,** Survival of HupT3 cells, quantified by firefly luciferase assay, upon concurrent knockout of *RELA* and *TFAP4* and coculture with MSLN CAR T or UTD control cells for 24 hours ($n = 3$; Dunnett test). *, $P < 0.05$; **, $P < 0.01$; ***, $P < 0.001$; ****, $P < 0.0001$.

TFAP4 and NFκB, we used Enrichr analyses and found an enrichment of p65-binding sites in the top upregulated genes following TFAP4 knockout, as well as enrichment in the TNFα signaling pathway (**Fig. 6D**; Supplementary Table S4; refs. 35–37). Furthermore, HupT3 cells lacking TFAP4 expression showed reduced sensitivity to FASL and TRAIL but not to gemcitabine (**Fig. 6E**; Supplementary Fig. S6C). Because p65 can subvert apoptotic pathways downstream of both FASL and TRAIL, reduced sensitivity to these death receptor ligands indicates altered p65 activity in the context of TFAP4 loss.

To directly test the importance of p65 downstream of TFAP4 loss, we generated double knockouts (Supplementary Fig. S6D). In consonance with our prior findings, concurrent deletion of TFAP4 and a control locus conferred CAR T-cell resistance. However, concurrent knockout of TFAP4 and p65 ablated the effect of TFAP4 depletion to enhance tumor cell survival, suggesting that p65 is necessary downstream of TFAP4 loss to confer MSLN CAR T-cell resistance (**Fig. 6F**). Together, these observations suggest a model in which TFAP4 loss licenses increased p65 activity, promoting an ISG-tolerant cell state and ultimately reduced CAR T-cell sensitivity.

Discussion

Despite the success of CAR T-cell therapy in B-cell malignancies, clinical response to CAR-based therapies in non–B-cell–derived tumors has been disappointing to date. Significant effort has been focused on improving CAR T-cell function, including strategies to generate CAR T cells that traffic to tumor sites more effectively, exhibit a balance of effector and memory-like states, resist immunosuppressive microenvironments, and maximally target tumor cells while sparing healthy tissue (22).

In addition to T-cell–centric studies, investigation of tumor cell–intrinsic mechanisms of CAR T-cell evasion are likely to inform

therapeutic application and outcome. Recently, other groups have also used genome scale genetic screens to identify tumor-intrinsic mechanisms of resistance to CAR T-cell therapy. Specifically, resistance to CD19-targeted CAR T-cell therapy in acute lymphoblastic leukemia was linked to deficiency in FAS and TRAIL death receptor circuitry that rendered tumor cells less sensitive to CAR T-mediated cytotoxicity despite maintenance of CD19 expression (19, 21). Furthermore, the IFN gamma receptor IFNγR was identified in a genome scale screen in glioblastoma cell lines as a mediator of CAR T-cell sensitivity in multiple solid tumor cell lines (20).

In contrast with FASL, TRAIL, and IFNγ, which are generally thought to promote T-cell–mediated killing, multiple studies have identified TNFα as a mediator of tumor cell survival in the context of TCR-based immune killing. For example, a screen using Pmel-1–redirected T cells and the B16F10 murine melanoma cell line identified multiple members of the TNF/NFκB pathway, including *RELA* (p65) as mediators of T-cell evasion (28). Another genome-scale CRISPR-Cas9 screen using human MART1^{+} melanoma cells and MART1-specific CD8 T cells reported depletion of multiple TNF signaling components, including *TRADD, TRAF2, TAK1*, and *cIAP1* (38). Furthermore, others found that SMAC mimetics, which inhibit IAP proteins, sensitized B-ALL cells to CD19 CAR T-cell therapy in a large-scale compound screen, suggesting that TNF/NFκB signaling promotes tumor cell survival in the context of CAR T cells as well.

Together these studies suggest that tumor-intrinsic cell states exert a meaningful influence on the ability of T cells, including CAR T cells, to effectively kill. To build upon and extend these findings in the context of PDAC, an indication with profound unmet need, we performed systematic functional genetic screens and uncovered multiple antigen-independent and -dependent modes of resistance and sensitivity to MSLN CAR T-cell therapy. Our findings suggest that the primary path to MSLN downregulation at the cell surface is loss of GPI anchor machinery. The majority of factors responsible for GPI anchor biosynthesis and transfer to the nascent protein scored strongly in both the HupT3 and KP4_MSLN screens, evidencing the importance of this pathway. In addition to the GPI anchor pathway, we identified multiple other antigen-dependent hits. Specifically, we showed that loss of the SNRPA splicing factor also reduced MSLN surface expression and conferred resistance to MSLN CAR therapy. Members of the adaptor protein complex (AP-2) AP2M1 and AP2S1, involved in clathrin-mediated endocytosis, also scored strongly in the HupT3 screen, as did dynamin 2 (DNM2), a related enzyme that facilitates membrane fission during endocytosis. Knockout of AP2M1 in HupT3 cells caused loss of MSLN expression, suggesting that defects in clathrin-mediated endocytosis could be another mode of antigen loss and MSLN CAR T-cell evasion.

SMARCA4, an ATPase component of the SWI/SNF chromatin remodeling complex, and *PGD*, a dehydrogenase in the pentose phosphate shunt that converts 6-phosphogluconate into ribulose 5-phosphate, also scored highly in the HupT3 screen and validated individually in coculture time courses. Knockout of these hits induced minor, and in the case of PGD, inconsistent changes in MSLN surface expression. Further work is needed to determine whether these changes in MSLN expression impact MSLN CAR T-cell sensitivity or if loss of these genes induces antigen-independent modes of evasion.

Our studies also uncovered tumor-intrinsic modes of CAR T-cell evasion that did not alter MSLN expression at the cell surface. In keeping with previous CAR T-cell resistance screens, our HupT3 screen highlighted the FAS/FADD death receptor pathway as a key mediator of MSLN CAR T-cell killing and emphasized the importance of this pathway for maintaining PDAC cell sensitivity to CAR T cells. Our work also highlighted the importance of NFκB in promoting CAR T-cell escape, as loss of *RELA* (p65) promoted marked sensitivity to MSLN CAR T cells whereas activation of NFκB via *NFKBIA* (IκBα) loss conferred a significant survival advantage. Furthermore, neutralization of TNFα, which activates the NFκB pathway in this context, reduced tumor cell survival upon CAR T-cell coculture, supporting the idea that NFκB pathway activation promotes CAR T-cell escape. We acknowledge that TNFα also induces cell death in some contexts, emphasizing that these findings relate to the context of CAR T-cell therapy in pancreatic cancers. Together, these findings extend previous work, indicating the importance of TNF signaling in evasion of T-cell killing, to the context of CAR T-cell therapy. Furthermore, because the HupT3 screen was designed to enrich for positively selected candidates, the consistent depletion of multiple NFκB pathway members suggests the importance of this pathway for CAR T-cell evasion in PDAC cells; however, it will be important to validate these depleted candidates in future work. Our work also suggests that therapeutically manipulating death receptor signaling away from NFκB-mediated survival and toward FADD-mediated death may be a promising strategy to sensitize PDAC cells to CAR T-cell killing. Indeed, prior analyses showed a significant correlation between a death receptor gene expression signature and response to CD19-directed CAR T-cell therapy, suggesting that these genes broadly modulate CAR T-cell responses (21). Among the other genes identified in these studies, we failed to find correlations with their expression and response to CD19-directed CAR T-cell studies, suggesting that these genes are likely relevant in the pancreatic cancer context.

In addition to the death receptor pathways, the HupT3 screen identified previously unrecognized mediators of antigen-independent CAR T-cell resistance. We showed that loss of INTS12, a member of the Integrator complex, conferred resistance to MSLN CAR T cells without affecting MSLN surface expression. Integrator exhibits myriad functions in regulating both the noncoding and coding transcriptome (39). Of the 18 members of this complex, *INTS12* is the only gene that scored highly in the HupT3 screen, indicating that this protein may function independently of the complex to mediate CAR T-cell sensitivity. However, data from the cancer cell dependency map indicate that many of the integrator complex components are essential in HupT3 cells, meaning that their knockout may have reduced cell fitness and that cells lacking these integrator proteins may have dropped out of the screen (29, 30). As such, additional work is needed to delineate the function of INTS12 from the function of the Integrator complex as it relates to MSLN CAR T-cell resistance.

We showed that oncogenic transcription factor TFAP4 exerts a broad impact on MSLN CAR T-cell cytotoxicity. Modulation of TFAP4 also affected HupT3 sensitivity to CAR T cells targeting EGFR, supporting the antigen independence of TFAP4-mediated CAR evasion and sensitization. We also tested the effect of TFAP4 manipulation in 3 additional PDAC cell lines; although TFAP4 overexpression was consistently detrimental to tumor cell survival, the impact of TFAP4 loss was variable across cell lines. This inconsistency may be attributed to differences in assay optimization, CAR design, or tumor antigen expression.

Investigating the mechanism downstream of TFAP4, we used altered IFN signatures to identify the NFκB transcription factor p65 as being a vital mediator of MSLN CAR T-cell resistance. These observations support the importance of TNF signaling and NFκB activity in resistance to T-cell killing (27). Additional work will be

required to determine how TFAP4 loss affects p65 activity, as well as the specific p65 targets that affect CAR T-cell sensitivity.

Taken together, these studies provide insight into the landscape of tumor-cell intrinsic mechanisms of MSLN CAR T-cell therapy resistance and sensitivity in PDAC. The identification and investigation of antigen-independent modes of CAR T evasion may be broadly applicable to CAR T-cell therapies redirected toward non-MSLN antigens. Finally, these observations support the existence of tumor-intrinsic cell states that could affect the clinical success of CAR T-cell therapy for solid tumors.

Authors' Disclosures

J.G. Doench reports personal fees from Pfizer, BioNTech, Sangamo, Tango Therapeutics, Abata Therapeutics, and Microsoft Research outside the submitted work. N.D. Mathewson reports grants from American Cancer Society and NIH education loan repayment program during the conduct of the study; personal fees from Immunitas Therapeutics and Asher Biotherapeutics outside the submitted work; a patent for PCT/US18/060857 issued to Dana-Farber Cancer Institute, PCT/US2020/047627 issued to Massachusetts Institute of Technology, and PCT/US2021/062484 issued to Asher Biotherapeutics. K.W. Wucherpfennig reports grants from NIH/NCI during the conduct of the study; personal fees from TScan Therapeutics, TCR2, Immunitas Therapeutics, SQZ Biotech, Bisou Bioscience Company, DEM BioParma, and Nextech Invest outside the submitted work. M.V. Maus reports personal fees from 2Seventy Bio outside the submitted work. W.C. Hahn reports grants from NCI during the conduct of the study and other support from Thermo Fisher Scientific, MPM, Solasta Ventures, KSQ Therapeutics, Frontier Medicines, Tyra Biosciences, Serinius Biosciences, Function Oncology, Jubilant Therapeutics, RAPPTA Therapeutics, and Calyx outside the submitted work. No disclosures were reported by the other authors.

Authors' Contributions

K.R. Hagel: Conceptualization, data curation, formal analysis, validation, investigation, writing–original draft, writing–review and editing. **R. Arafeh:** Supervision, investigation. **S. Gang:** Investigation. **T.E. Arnoff:** Investigation. **R.C. Larson:** Resources, methodology. **J.G. Doench:** Resources, supervision. **N.D. Mathewson:** Resources. **K.W. Wucherpfennig:** Conceptualization, resources. **M.V. Maus:** Conceptualization, resources. **W.C. Hahn:** Conceptualization, resources, supervision, funding acquisition, writing–review and editing.

Acknowledgments

This work was supported in part by the Weizmann Institute of Science—National Postdoctoral Award Program for Advancing Women in Science (to R. Arafeh) and NCI grants U01 CA176058 and U01 CA224146 (to W.C. Hahn). The authors thank Carl June for sharing the lentiviral backbone used to generate their MSLN CAR construct.

The publication costs of this article were defrayed in part by the payment of publication fees. Therefore, and solely to indicate this fact, this article is hereby marked "advertisement" in accordance with 18 USC section 1734.

Note

Supplementary data for this article are available at Cancer Research Online (http://cancerres.aacrjournals.org/).

Received July 13, 2022; revised October 18, 2022; accepted December 21, 2022; published first December 22, 2022.

References

1. Brentjens R, Davila ML, Riviere I, Park J, Wang X, Cowell LG, et al. CD19-targeted T cells rapidly induce molecular remissions in adults with chemotherapy-refractory acute lymphoblastic leukemia. Sci Transl Med 2013;5:177ra38.
2. Lee DW, Kochenderfer JN, Stetler-Stevenson M, Cui YK, Delbrook C, Feldman SA, et al. T cells expressing CD19 chimeric antigen receptors for acute lymphoblastic leukaemia in children and young adults: a phase 1 dose-escalation trial. Lancet 2015;385:517–28.
3. Park JH, Rivière I, Gonen M, Wang X, Sénéchal B, Curran KJ, et al. Long-term follow-up of CD19 CAR therapy in acute lymphoblastic leukemia. N Engl J Med 2018;378:449–59.
4. Turtle CJ, Hanafi L-A, Berger C, Gooley TA, Cherian S, Hudecek M, et al. CD19 CAR–T cells of defined $CD4^+$:$CD8^+$ composition in adult B-cell ALL patients. J Clin Invest 2016;126:2123–38.
5. Rahib L, Wehner MR, Matrisian LM, Nead KT. Estimated projection of US cancer incidence and death to 2040. JAMA Network Open 2021;4:e214708.
6. Siegel RL, Miller KD, Fuchs HE, Jemal A. Cancer statistics, 2022. CA Cancer J Clin 2022;72:7–33.
7. da Costa WL, Oluyomi AO, Thrift AP. Trends in the incidence of pancreatic adenocarcinoma in all 50 United States examined through an age–period–cohort analysis. JNCI Cancer Spectr 2020;4:pkaa033.
8. Kleeff J, Korc M, Apte M, La Vecchia C, Johnson CD, Biankin AV, et al. Pancreatic cancer. Nat Rev Dis Primers 2016;2:1–22.
9. Dorman K, Heinemann V, Kobold S, von Bergwelt-Baildon M, Boeck S. Novel systemic treatment approaches for metastatic pancreatic cancer. Expert Opin Investig Drugs 2022;31:249–62.
10. Klampatsa A, Dimou V, Albelda SM. Mesothelin-targeted CAR T-cell therapy for solid tumors. Expert Opin Biol Ther 2021;21:473–486.
11. Hassan R, Thomas A, Alewine C, Le DT, Jaffee EM, Pastan I. Mesothelin immunotherapy for cancer: ready for prime time? J Clin Oncol 2016;34:4171–9.
12. Bera TK, Pastan I. Mesothelin is not required for normal mouse development or reproduction. Mol Cell Biol 2000;20:2902–6.
13. Thistlethwaite FC, Gilham DE, Guest RD, Rothwell DG, Pillai M, Burt DJ, et al. The clinical efficacy of first-generation carcinoembryonic antigen (CEACAM5)-specific CAR T cells is limited by poor persistence and transient pre-conditioning-dependent respiratory toxicity. Cancer Immunol Immunother 2017;66:1425–36.
14. Wang Z, Chen W, Zhang X, Cai Z, Huang W. A long way to the battlefront: CAR T-cell therapy against solid cancers. J Cancer 2019;10:3112–23.
15. Beatty GL, Haas AR, Maus MV, Torigian DA, Soulen MC, Plesa G, et al. Mesothelin-specific chimeric antigen receptor mRNA-engineered T cells induce antitumor activity in solid malignancies. Cancer Immunol Res 2014;2:112–20.
16. Beatty GL, O'Hara MH, Lacey SF, Torigian DA, Nazimuddin F, Chen F, et al. Activity of mesothelin-specific chimeric antigen receptor T cells against pancreatic carcinoma metastases in a phase 1 trial. Gastroenterology 2018;155:29–32.
17. Haas AR, Tanyi JL, O'Hara MH, Gladney WL, Lacey SF, Torigian DA, et al. Phase I study of lentiviral-transduced chimeric antigen receptor-modified T cells recognizing mesothelin in advanced solid cancers. Mol Ther 2019;27:1919–29.
18. Rosenberg S. Phase I/II study of metastatic cancer using lymphodepleting conditioning followed by infusion of anti-mesothelin gene engineered lymphocytes [Internet]. clinicaltrials.gov; 2019. Report No.: results/NCT01583686. Available from: https://clinicaltrials.gov/ct2/show/results/NCT01583686.
19. Dufva O, Koski J, Maliniemi P, Ianevski A, Klievink J, Leitner J, et al. Integrated drug profiling and CRISPR screening identify essential pathways for CAR T-cell cytotoxicity. Blood 2020;135:597–609.
20. Larson RC, Kann MC, Bailey SR, Haradhvala NJ, Llopis PM, Bouffard AA, et al. CAR T-cell killing requires the IFNγR pathway in solid but not liquid tumours. Nature 2022;604:563–70.
21. Singh N, Lee YG, Shestova O, Ravikumar P, Hayer KE, Hong SJ, et al. Impaired death receptor signaling in leukemia causes antigen-independent resistance by inducing CAR T-cell dysfunction. Cancer Discov 2020;10:552–67.
22. Kyte JA. Strategies for improving the efficacy of CAR T cells in solid cancers. Cancers 2022;14:571.
23. Lim WA, June CH. The principles of engineering immune cells to treat cancer. Cell 2017;168:724–40.
24. Choi BD, Yu X, Castano AP, Bouffard AA, Schmidts A, Larson RC, et al. CAR T cells secreting BiTEs circumvent antigen escape without detectable toxicity. Nat Biotechnol 2019;37:1049–58.
25. Edgar R, Domrachev M, Lash AE. Gene expression omnibus: NCBI gene expression and hybridization array data repository. Nucleic Acids Res 2002;30:207–10.

26. Doench JG, Fusi N, Sullender M, Hegde M, Vaimberg EW, Donovan KF, et al. Optimized sgRNA design to maximize activity and minimize off-target effects of CRISPR-Cas9. Nat Biotechnol 2016;34:184–91.
27. Manguso RT, Pope HW, Zimmer MD, Brown FD, Yates KB, Miller BC, et al. In vivo CRISPR screening identifies Ptpn2 as a cancer immunotherapy target. Nature 2017;547:413–8.
28. Pan D, Kobayashi A, Jiang P, Ferrari de Andrade L, Tay RE, Luoma AM, et al. A major chromatin regulator determines resistance of tumor cells to T-cell–mediated killing. Science 2018;359:770–5.
29. Behan FM, Iorio F, Picco G, Gonçalves E, Beaver CM, Migliardi G, et al. Prioritization of cancer therapeutic targets using CRISPR-Cas9 screens. Nature 2019;568:511–6.
30. Meyers RM, Bryan JG, McFarland JM, Weir BA, Sizemore AE, Xu H, et al. Computational correction of copy number effect improves specificity of CRISPR-Cas9 essentiality screens in cancer cells. Nat Genet 2017;49:1779–84.
31. Szklarczyk D, Franceschini A, Wyder S, Forslund K, Heller D, Huerta-Cepas J, et al. STRING v10: protein–protein interaction networks, integrated over the tree of life. Nucleic Acids Res 2015;43:D447–452.
32. Wong MM-K, Joyson SM, Hermeking H, Chiu SK. Transcription factor AP4 mediates cell fate decisions: to divide, age, or die. Cancers 2021;13:676.
33. Benci JL, Xu B, Qiu Y, Wu T, Dada H, Victor CT-S, et al. Tumor interferon signaling regulates a multigenic resistance program to immune checkpoint blockade. Cell 2016;167:1540–54.
34. Pfeffer LM. The role of nuclear factor κB in the interferon response. J Interferon Cytokine Res 2011;31:553–9.
35. Chen EY, Tan CM, Kou Y, Duan Q, Wang Z, Meirelles GV, et al. Enrichr: interactive and collaborative HTML5 gene list enrichment analysis tool. BMC Bioinf 2013;14:128.
36. Kuleshov MV, Jones MR, Rouillard AD, Fernandez NF, Duan Q, Wang Z, et al. Enrichr: a comprehensive gene set enrichment analysis web server 2016 update. Nucleic Acids Res 2016;44:W90–7.
37. Xie Z, Bailey A, Kuleshov MV, Clarke DJB, Evangelista JE, Jenkins SL, et al. Gene set knowledge discovery with enrichr. Current Protocols. 2021; 1:e90.
38. Vredevoogd DW, Kuilman T, Ligtenberg MA, Boshuizen J, Stecker KE, de Bruijn B, et al. Augmenting immunotherapy impact by lowering tumor TNF cytotoxicity threshold. Cell 2019;178:585–99.
39. Kirstein N, Gomes Dos Santos H, Blumenthal E, Shiekhattar R. The integrator complex at the crossroad of coding and noncoding RNA. Curr Opin Cell Biol 2021;70:37–43.